Emission and Propagation Mechanisms of PD Pulsesfor UHF and Traditional Electrical Measurements

S. M. Hoek[1], M. Koch[2], M. Heindl[3]

[1]OMICRON electronics GmbH, Klaus, Austria, [2]OMICRON Energy Solutions GmbH, Berlin, Germany, [3]University of Stuttgart, Stuttgart, Germany
Stefan.Hoek@omicron.at

Abstract: Partial Discharge measurements are considered as a powerful technique for testing and monitoring the condition of high-voltage insulations sinceit serves as an early breakdown indicator. In the present contribution, the authors describe the fundamentally different propagation mechanisms of electrical impulses in the conventional measurement frequency range according IEC 60270 and in the ultra-high frequency range. Electromagnetic field simulation and measurements in GIS are used to elaborate the signal propagation mechanisms. The low-frequency components of the PD signals propagate mainly via the conductor, whereas the high-frequency components (UHF signals) are radiated as electromagnetic waves. The sensitivity and spectrum of the measurement depends strongly on the geometric position of the PD, damping and resonances of the propagation path, and the frequency response of the receiver. Due to their different, complex propagation mechanisms, apparent charge level after IEC 60270 and UHF antenna peak voltage cannot be compared directly nor can frequency spectra be easily used for deriving information about the physical nature of the defect.

Index Terms: Partial discharges PD, ultra high frequency UHF, IEC 60270, wave and conductor guided dispersion, electromagnetic field simulation, gas insulated switchgear GIS.

1. Introduction

An important and worldwide accepted element for acceptance tests, on-site diagnostics and on-line monitoring of HV insulation systems is the partial discharge (PD) measurement[1]. This is also reflected in numerous standards. Partial discharges are local electrical discharges that partially break down the high-voltage (HV) insulation [2]and generate electric impulses as well as electromagnetic waves in a broad frequency spectrum due to their short rise time and duration[3]. As an example, for protrusions rise times of impulses of 35 ps, corresponding to frequencies up to 10 GHz, have been verified by[4]. Measurement and detection of PD is performed with different methods involving different propagation paths, propagation mechanisms and sensor principles which result in divergent transfer behavior. The traditional setup according to IEC 60270 uses band pass filters with a center frequency of some 100 kHz, aiming to measure in a frequency range less subject to external disturbances which are typically radiating in a broad frequency spectrum. For higher center frequencies of some 100 MHz, a fundamentally different nature of the disturbances can be expected; resulting often in a more narrowband signal character at the measurement location[5], [6]. Table 1 compares basic features of electrical, low frequency measurements to them at UHF frequency.

Disturbances and internal discharges often have different frequency spectra. This can be used to discriminate between them during on-site and on-line measurements by choosing a suitable measurement frequency or by combining the conventional and the UHF technique. However, there are general uncertainties related to the comparability of the UHF measurements

Received: February 29th, 2012. Accepted: October 27th, 2012

to conventional IEC conformant tests[7]. For example, during CIGRÉ Session 2008 the Special Reporter of Study Committee D1 asked the question: "How can the relation between the conventional PD measurement and the UHF measurement be determined and generalized?" [8].

Table 1. Characteristics of electrical and UHF measurements in comparison

	Electrical measurement (IEC 60270)	UHF measurement
Propagation	Displacement current	Electromagnetic field
Sensor	Coupling capacitor	Antenna
Frequency	100 kHz – some MHz	100 – 2000 MHz

In the present contribution, the authors detail the fundamentally different propagation mechanisms of electric impulses based on Maxwell's law of total current. Simulation results of PD signal propagation in gas-insulated switchgear (GIS) illustrate graphically the complex and very geometry-sensitive transfer function of UHF signals. This helps to understand the physical nature of impulse propagation for different frequency ranges and allows drawing conclusions on the information obtained from various test methods.

2. Theory of Impulse Propagation

A. Maxwell's Law of Total Currents

For describing the principles of electromagnetic impulse propagation, one may start with the famous equations of Maxwell. An electrical field $E(t)$ generates a current density $J(t)$ as a sum of conduction and displacement currents, where σ_0 is the volume conductivity of that material. From (1) it can be concluded that

- Electrical conduction consists of two phenomena, where one is related to a conductor and the other to an insulating medium existing between the conductors.
- The second phenomenon, displacement current, is particularly present for fast variations of *d/dt*, that is, for high frequencies and, together with (2),leads to electromagnetic wave propagation.

$$\nabla \times H(t) = J(t) = \sigma_0 E(t) + \frac{dD(t)}{dt} \tag{1}$$

$$\nabla \times E(t) = -\frac{dB(t)}{dt} \tag{2}$$

B. Signal Propagation for Low Frequencies

The propagation of PD signals with low frequencies in conductors usually takes place by conduction currents. In a conductor, the surrounding magnetic field is closed. The electric field has its origin on the conductor surface and spreads radially. Neither the H-field nor the E-field has components in the direction of propagation. This corresponds to the definition of propagation of the TEM-mode, able to propagate from DC to very high frequencies.

C. Electromagnetic Wave Propagation

For UHF frequencies, the conductive structure works increasingly as an antenna, whose cut-off frequency depends on the dimensions especially close around the PD source. Correspondingly, the structure of the PD source influences the PD signal.

3. Simulation of PD Signal Propagation in GIS

A. Simulation Model

For investigating characteristics of the two common PD measurement principles, a simulation model of a GIS was created using CST Microwave Studio (MWS) software package. MWS uses the finite integration technique (FIT) to solve electromagnetic field problems in time domain[10]. It is suitable to simulate electromagnetic wave propagation mechanisms through air and wire within electrically large structures like GIS. Figure 1 shows an overview of the simulation arrangement. The model consists of an evacuated tube of 7.4 m length with a diameter of 55 cm and a centered inner conductor tube with 16 cm diameter. The inner conductor is held in position by three epoxy resin spacers with permittivity $\varepsilon_r = 4.0$. Both ends of the GIS are terminated with so-called waveguide ports which are adapted to the characteristic wave impedance of the arrangement. This technique provides absorption of wave energy and inhibits total reflection at both ends of the structure. Otherwise reflections would keep electromagnetic waves propagating through the lossless arrangement over and over again without decreasing of the overall field energy, which would be an unrealistic boundary condition.

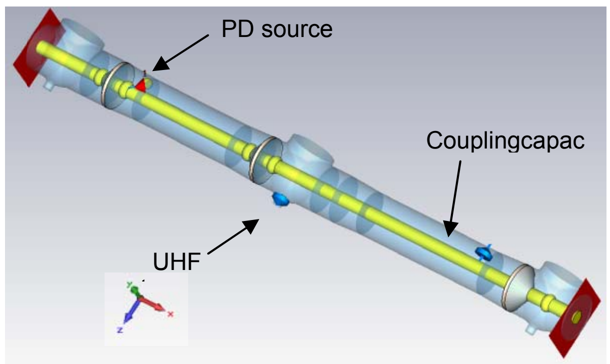

Figure 1. GIS model overview in CST MWS

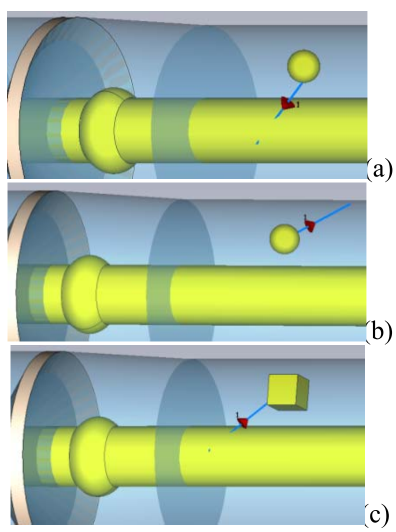

Figure 2.PD source configurations: (a) spherical shape, inner conductorfed, (b) spherical shape, outer conductorfed and (c) cubical shape, inner conductorfed

The injection of PD pulses into the inner conductor of the GIS, i.e. simulation of a PD source, was carried out by an additional insulated spherical (respectively cubical) conductor between the inner and outer conductor (Figure 2 A pulse voltage source connects the sphere or cube to the GIS and injects a PD impulse of Gaussian shape with 1 ns rise time and a corresponding frequency range up to 1Ghz. This composition fulfils two purposes:

- Radiation of electromagnetic waves as they are caused by real PD sources
- Injection of a “PD current” into the conducting part of the GIS

Decoupling of the PD signals is done in two different ways. Firstly, a coupling capacitor acquires the signals on the GIS inner conductor and follows the measurement procedure as described in IEC 60270. Secondly, with the UHF method, the PD signals are detected in the UHF frequency range with disk antennas.In the simulation, both for the conventional coupling capacitoras well for the UHF antenna, PD signals are recorded by monitoring voltage and current through lumped elements.

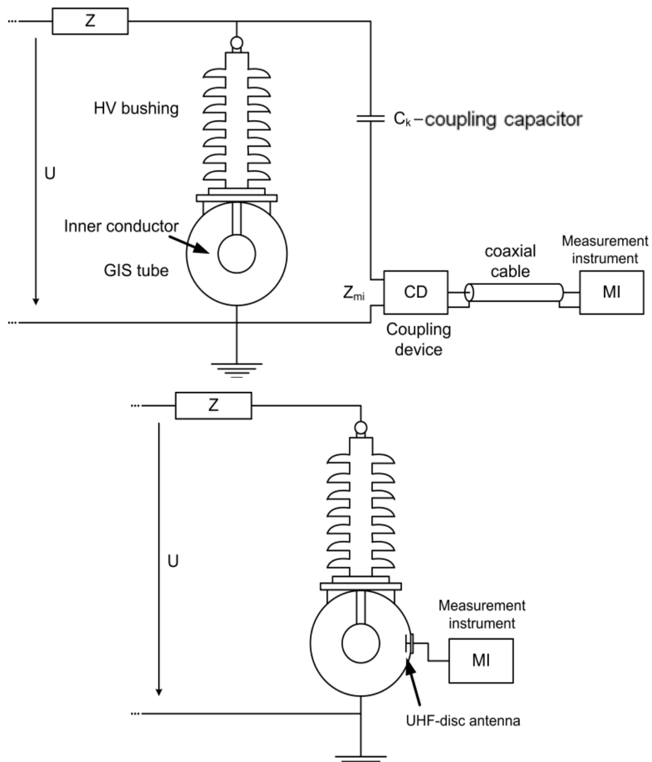

Figure 3. Coupling of PD signals with coupling capacitor accordingto the IEC 60270 (above) and with disc-type antenna in the UHF range (below)

B. Electromagnetic Field Propagation

Figure 4 illustrates the propagation of the electromagnetic field initiated by the PD impulse in GIS by showing the electrical field strength. After a time of 8 ns, the UHF sensor is reached. After 17 ns, the impulse is at the PD coupling capacitor. Thereafter it leaves the GIS through the waveguide ports. The electromagnetic field distribution is non-uniform. The impulse is oscillating right from the beginning due to the electrical features of the close surrounding of the PD source.

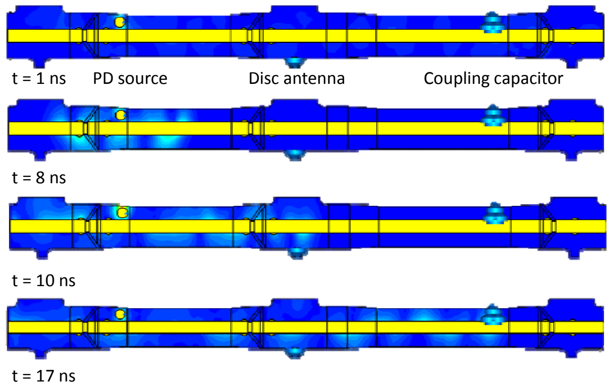

Figure 4. Electromagnetic field propagation in y-plane (side view)

With the view from below on the propagating electromagnetic wave (Figure 5), the field distribution is much more symmetrical since the PD source is in central position behind the inner conductor. Here, the signal reflection at the spacers, caused by their different wave impedance, is visible at t = 23 ns. The original PD impulse has already left the calculation space, whereas the reflected parts form an additional maximum at the location of the coupling capacitor.

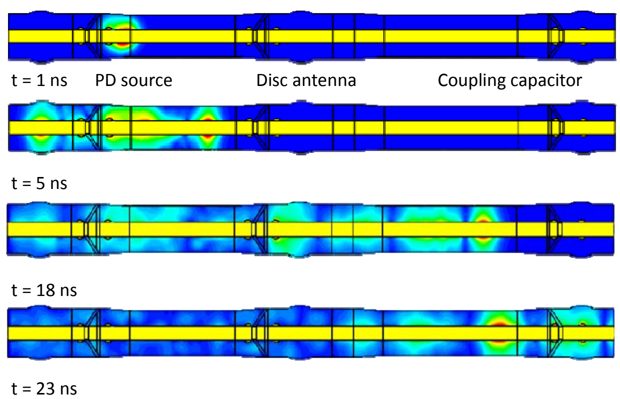

Figure 5. Electromagnetic field propagation in z-plane (bottom view)

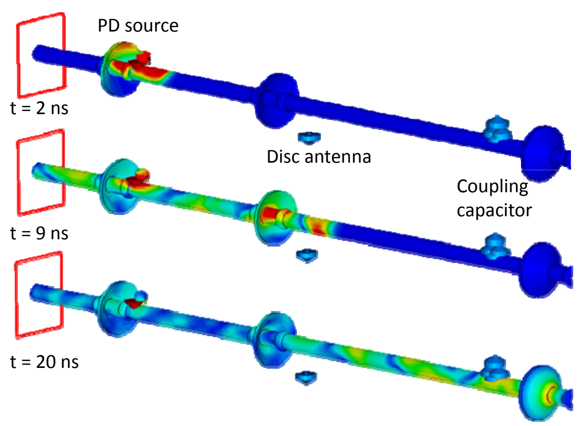

Figure 6. Surface current propagation along the metallic parts of the GIS

With the surface current distribution, calculated for the inner conductor and spacers, Figure 6, again the non-uniform field and current distribution is emphasized. While measuring at high frequencies, any change in position of PD source or sensor will have a large effect on the measured signals.

C. Wave Modes in GIS

Three different types of wave modes propagate in cavities with conductive boundaries like GIS [6]: The TM_{mn}-mode ($H_X = 0$), the TE_{mn}-mode ($E_X = 0$) and the TEM-mode ($H_X = 0$, $E_X = 0$), where m and n mark the different types of wave modes. Every wave mode, except the TEM-mode, has its own critical frequency (f_c). TE or TM modes propagate at frequencies above their own critical or cut-off-frequency (f_c).

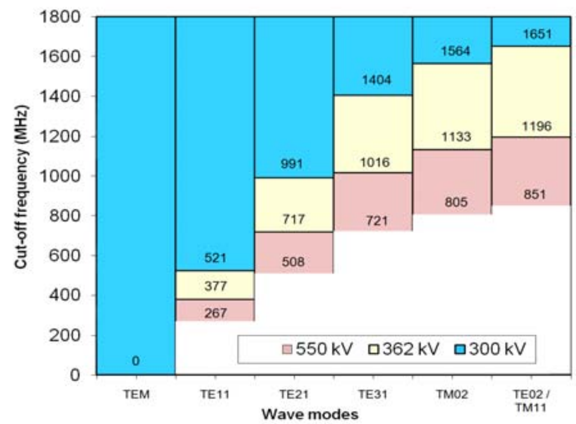

Figure 7. Cut-off frequencies (fco) within a GIS for 300 kV, 362 kV and 550 kV [9]

Additionally to the basic TEMsignal propagation mode, higher order modes (TE- and TM-mode) may propagate depending on the geometry. The higher order modes propagate only above their cut-off frequencies (f_{co}). InFigure 7, the cut-off frequencies of the first wave modes are shown for three different diameters, respectively different types of GIS.

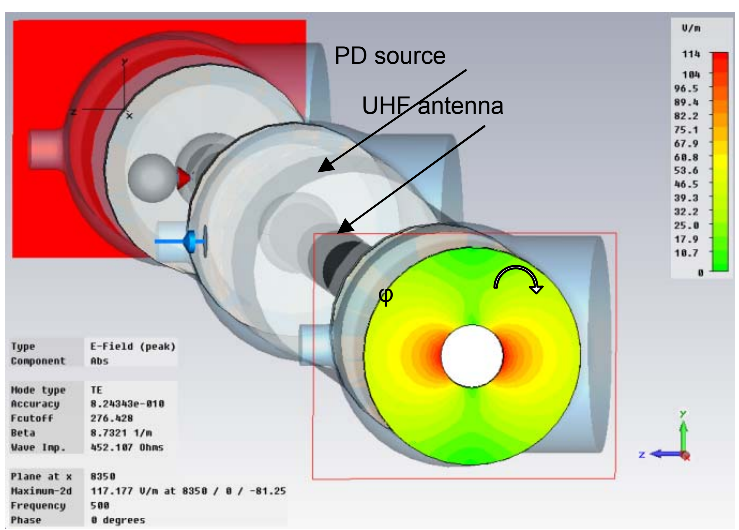

Figure 8. Electrical field distribution of TE11 wave mode inside GIS

Each of this higher order modes are reflected at discontinuities, generate interference patterns and standing waves (resonances), and are damped by skin effect and lossy dielectric material. What is finally picked up at the broadband UHF PD sensor (built into the GIS) is the complex superposition of all modes, which result in a frequency spectrum with various resonances and frequency bands with highly different measurement sensitivity. As a result, the sensitivity of a PD-sensor is significantly dependent on the specific geometry of the signal transmission path between PD-sensor and PD-source[11]. In the terminology of radio technology, the GIS can be described as a heavily overmoded waveguide [12].

The TE and TM mode (often called higher modes) have H- and E-field components in the propagation direction and show an unsymmetrical field distribution (Figure 8,

Figure 9 in the transversal plain[13]. This field distribution explains the transmission of the PD signal from source to sensor as a function of the angle φ between source positions in relation to the sensor position.

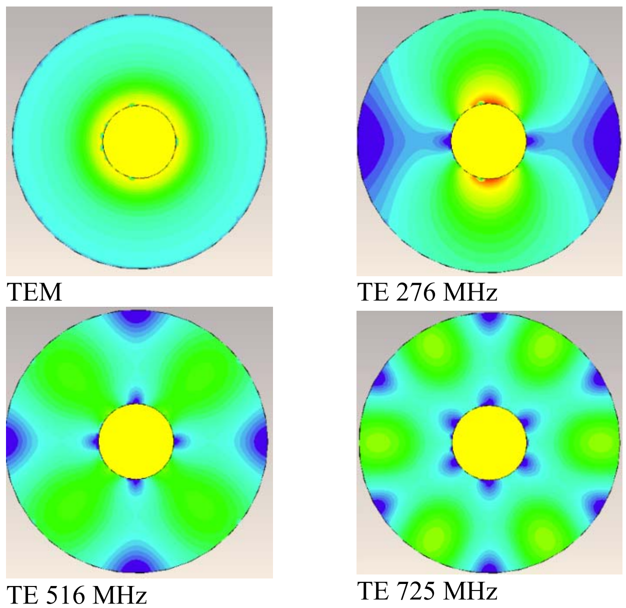

Figure 9. Transversal electrical mode propagation in GIS

The analysis of the energy distribution of the different modes over frequency range is shown in

Figure 10. It reflects the importance of the higher modes for the signal propagation in the UHF range. Due to the skin effect and losses at spacers, the propagating signals are damped; these effects are frequency-dependent.

The complexity is further increased by considering the frequency dependence of the group velocity (v_g) of the TE- / TM-wave modes especially around their cut-off-frequency [9].

$$v_g\ (f) = c_0 \cdot \sqrt{1-\left(\frac{f_{co}}{f}\right)^2} = \sqrt{1-\left(\frac{f_{co}}{f}\right)^2 \Big/ (\varepsilon_0 \cdot \mu_0)} \tag{3}$$

These shown transfer mechanisms sum up to a complex spectrum which is measureableat the UHF sensors. Figure 11 (overall spectrum) shows the on-site measured spectrum at a 245 kV GIS. Measureable at the UHF sensors are additionally to the PD related spectrum the continuous waveform (CW) or narrowband sinusoidal disturbances (arrows in Figure 11) caused e.g. by broadcast system. The spectrum of the continuous waveforms (CW) only is shown in the low curve in Figure 11.

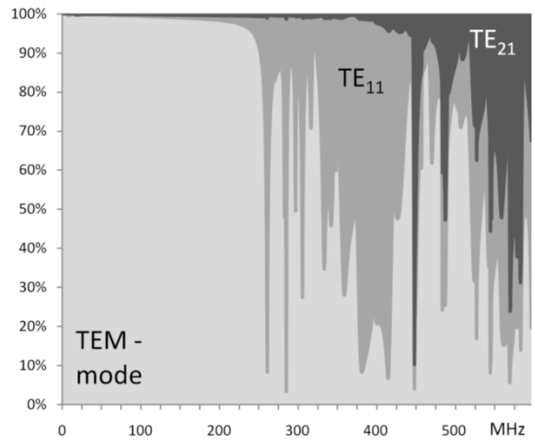

Figure 10. Share of the TEM-wave modes and higher modes ($TE_{11}$and TE_{21}) at the total transfer versus the frequency [14]

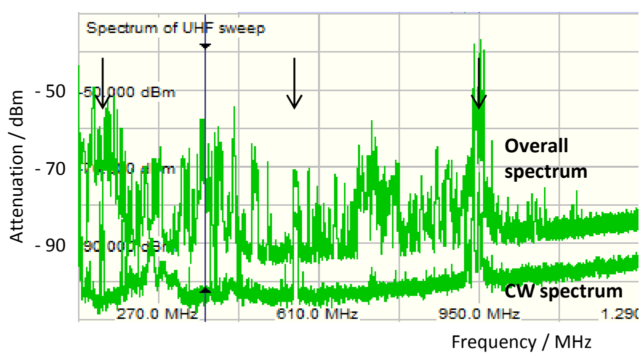

Figure 11. Measured spectrum in the GIS (upper line) and sinusoidalor continuous wave (CW) disturbance (lower line)

D. Influence of PD Source Position

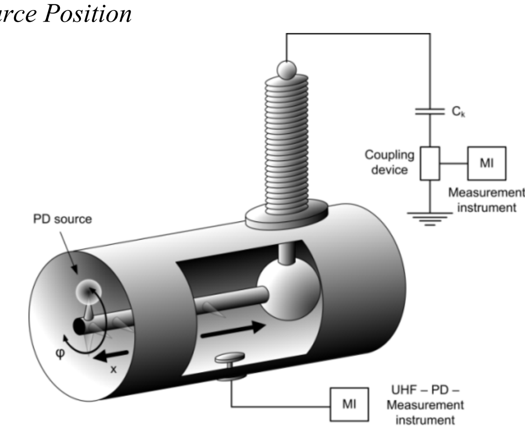

Figure 12. Detection of PD sources in GIS by conventional and UHF method.

In this section, the influence of the PD source position using the spherical structure on the measured signals is investigated Figure 2. The position of the PD source is defined by its x-position and angle φ within the yz-plane (Figure 12).First, the angle was varied while the x-position was constant. Figure 13shows apparent charge level and peak voltage picked up by the UHF antenna when the x-position of the PD source was kept constant and its angle φ was varied in steps of 90°. Again, the apparent charge level remains almost constant while the UHF peak voltage varies by almost 25%. This can be explained by the complex wave propagation mechanisms for signals in the UHF range [14].

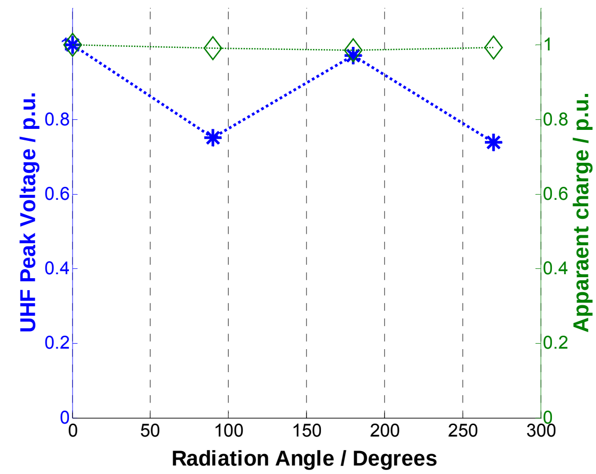

Figure 13. UHF peak voltage and apparent charge level vs. radiation angle of PD source

This effect is explainable by wave modes inside of the GIS. The field components in the direction of propagation of the TE- / TM-modes results in an angle dependence of the field distribution in the yz-plane as it is shown in Figure 13.

In further experiment simulations the PD source is modifided in the following way. The diameter of the PD source was decreased from 60 mm to 30 mm while the position of the sphere remained identical. Figure 14 shows the measurable UHF antenna peak voltage and apparent charge level when the diameter was varied.

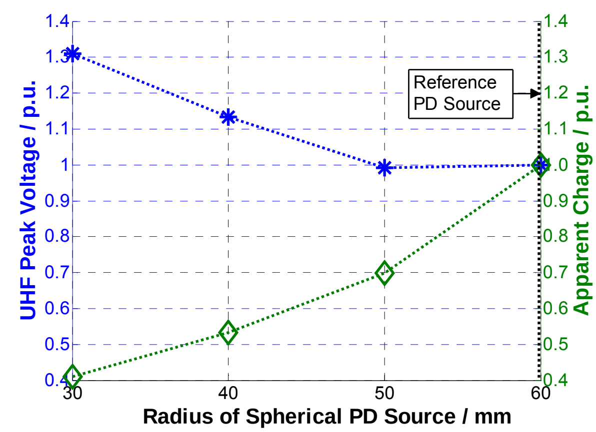

Figure 14. UHF peak voltage and apparent charge level vs. size PD source

Due to smaller clearances between PD source and conduction structure for enlarged radius, the capacitive coupling is increased. This leads to an increasing apparent charge level for extended radiuses. In contrast to that, the UHF peak voltage decreases for bigger sphere diameters, which can be explained by changed radiation characteristics.

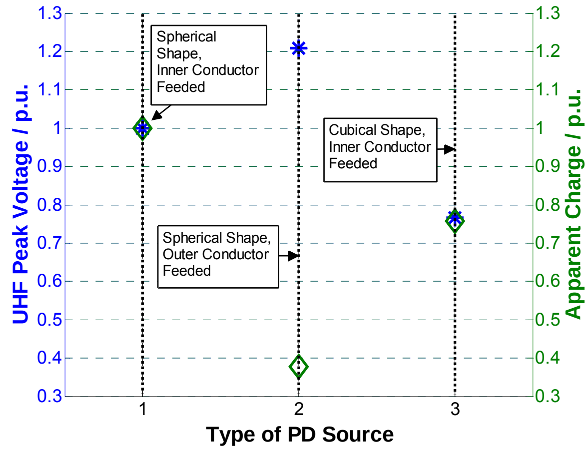

Figure 15. UHF peak voltage and apparent charge level for different PD source geometries

Figure 15 shows the measurable UHF antenna peak voltage and apparent charge level when the source shape type was varied according to Figure 2. Both the UHF antenna peak voltage and apparent charge level were normalised to source type 1.

The capacitance between sphere and outer conductor (type 1) is higher than the capacitance between sphere and inner conductor (type 2). Therefore the apparent charge level is reduced for source type 2. In contrast to this, the UHF antenna peak voltage is *increased* by the changed radiation characteristics. For PD source type 3, the circumstances are comparable to source type 1 which gives a corresponding UHF and apparent charge level.

4. Conclusions

The measurable signal spectrum (magnitude vs. frequency) depends directly on source geometry and location, structure of the test specimen, the used sensor and the measurement instrument. Figure 16 illustrates the propagation of PD signals from source to receiver. The originally very wide frequency spectrum of a Dirac-like discharge spark is modified by the electric characteristics of its close surroundings, the propagation path with its damping and resonances and finally by the frequency response of the measurement system. The receiver will detect only a fraction of the originally very wide frequency spectrum and the original amplitude.

- The low-frequency components of the PD signals propagate mainly via the conductor. It is expected that in electrically large setups the damping of the signal is not negligible during calibration and measurement.
- The high-frequency components (UHF signals) propagate through electromagnetic waves. The propagation is mainly influenced by the geometric circumstances.
- The sensitivity of the UHF measurement and its spectrum depends strongly on the geometric position of the PD, geometry of the source, damping and resonances of the propagation path and the frequency response of the receiver.
- Field simulation has been used as an appropriate tool for calculating PD signal propagation in HV apparatus.

UHF antenna peak voltage and apparent charge level cannot be compared directly. While the measureable apparent charge level of PD sources is mainly determined by the capacitive couplings of the structures and the conductor properties, the detectable UHF signal is influenced by the geometry of the GIS and source.

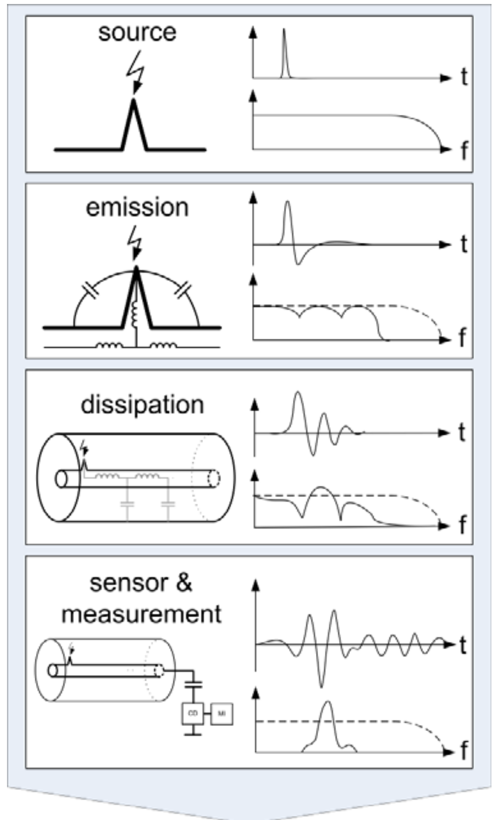

Figure 16. PD signal propagation and variation of time signals and frequency spectrum from source to receiver.

References

[1]. König and Y.N. Rao: "Partial Discharges in Electrical Power Apparatus", VDE 1993

[2]. IEC 60270, "High-voltage test techniques – Partial discharge measurement", Version 2000, 3rd Edition

[3]. M.D. Judd, S. Meijer and S. Tenbohlen, “Sensitivity check for RF PD detection for power transformers,” *IEEE Conference on Condition Monitoring and Diagnosis (CMD), Peking, China, April 21-24, 2008, paper No. K1-03*

[4]. A.J. Reid, M.D. Judd; "High Bandwidth measurement of Partial Discharge Pulses in SF6"; 14th ISH Beijing, China, August 25-29 2005; G-012

[5]. M.D. Judd, O. Farish, B.F. Hampton, "The Excitation of UHF Signals by Partial Discharges in GIS", *IEEE Transactions on Dielectrics and Electrical Insulation, Vol. 3 No. 2, April 1996*

[6]. S. Tenbohlen, S.M. Hoek, D. Denissov, S.M. Markalous, “Partial Discharge Measurement in the Ultra High Frequency (UHF) Range,” *IEEE Tr. on Dielectrics and Electrical Insulation, Vol. 15, No. 6/2008, pp. 1544-1552*

[7]. S.M. Hoek, S. Coenen, M. Bornowski, S Tenbolen: "Fundamental Differences of the PD Measurement according to IEC 60270 and in UHF range", *2008 International Conference on Condition Monitoring and Diagnosis, Beijing, China, April 21-24, 2008*

[8]. J. Densley et al. "Special Report for Group D1", Cigré Main Session 2008, online available at www.cigre.org

[9]. S.M. Hoek, U. Riechert, T. Strehl, K. Feser, and S. Tenbohlen, "New Procedures for Partial Discharge Localization in Gas-Insulated Switchgears in Frequency and Time Domain", ISH Ljubljana / Slovenia, August 2007

[10]. Munteanu, M. Timm, T. Weiland, “It’s About Time,” Microwave Magazine, *IEEE, vol. 11, issue 2, pp. 60–69, March 2010.*
[11]. G.J. Behrmann, S.M. Neuhold, R. Pietsch, „Results of UHF measurements in a 220-kV-GIS Substation during on-site commissioning tests; 10th ISH Montreal; August 1997
[12]. S.M. Hoek, S.M. Neuhold, "Tuned Medium-Band UHF PD Measurement system for GIS" 17th ISH Hannover, Germany, August 2011
[13]. R. Kurrer, K. Feser, "The Application of Ultra-High-Frequency Partial Discharge Measurements to Gas-Insulated Substations", *IEEE Transactions on Power Delivery, Vol. 13, No. 3, July 1998*
[14]. S.M. Hoek, M. Koch and M. Heindl, "Propagation Mechanisms of PD Pulses for UHF and Traditional Electrical Measurements" *IEEE Conference on Condition Monitoring and Diagnosis (CMD), Tokyo, Japan, Sept 06-11, 2010, paper No. C2-02*

Stefan Hoek is product manager for partial discharge measurement system and joined OMICRON, Austria in 2008. He studied electrical engineering at the University Stuttgart (Germany) and worked there as research assistant with focus on partial discharge detection and localization in GIS with help of measurements in the UHF range. Stefan Hoek is member of VDE ETG and CIGRE working group and published several papers.

Maik Koch leads the Product Management and Asset Expert team within Omicron Monitoring, Berlin. He studied electrical power engineering at various German universities and graduated as a PhD at the University of Stuttgart in Germany in 2008. In 2007, he joined Omicron. His field of expertise is condition assessment of HV assets by electrical, chemical and dielectric analysis methods. He wrote more than 70 scientific papers and contributes to working groups of CIGRE and IEEE dealing with subjects such as dielectric response testing, insulation ageing and on-line monitoring.

Maximilian Heindl received the Diploma degree in electrical engineering and information technology from the University of Stuttgart, Germany, in 2007 and joined the Institute of Power Transmission and High Voltage Technology, where he currently is doctoral research assistant. The focus of his work and research lies on high voltage related modeling of both high and low frequency problem types. Maximilian Heindl is member of CIGRE and VDE ETG and published several papers.